REPORT DOCUMENTATION PAGE

Form Approved
OMB No. 0704-0188

1. REPORT DATE *(DD-MM-YYYY)*	**2. REPORT TYPE**	**3. DATES COVERED** *(From - To)*
January 2014	Journal Article	January 2014-April 2014

4. TITLE AND SUBTITLE

Physics-based Scaling Laws for Confined and Unconfined Transverse Jets

5a. CONTRACT NUMBER
In-House

5b. GRANT NUMBER

5c. PROGRAM ELEMENT NUMBER

6. AUTHOR(S)

Forliti, D.J., Salazar, D.V., and Bishop, A.J.

5d. PROJECT NUMBER

5e. TASK NUMBER

5f. WORK UNIT NUMBER
Q09Z

7. PERFORMING ORGANIZATION NAME(S) AND ADDRESS(ES)

Air Force Research Laboratory (AFMC)
AFRL/RQRC
10 E. Saturn Blvd.
Edwards AFB, CA, 93524-7680

8. PERFORMING ORGANIZATION REPORT NO.

9. SPONSORING / MONITORING AGENCY NAME(S) AND ADDRESS(ES)

Air Force Research Laboratory (AFMC)
AFRL/RQR
5 Pollux Drive.
Edwards AFB, CA, 93524-7048

10. SPONSOR/MONITOR'S ACRONYM(S)

11. SPONSOR/MONITOR'S REPORT NUMBER(S)
AFRL-RQ-ED-JA-2014-106

12. DISTRIBUTION / AVAILABILITY STATEMENT
Approved for public release; distribution unlimited

13. SUPPLEMENTARY NOTES
Journal article published in the Experiments in Fluids, Vol. #56, Issue #36, Feb 2015.
PA Case Number: #14206; Clearance Date: 29 Apr 14.

14. ABSTRACT

An experimental study was conducted to explore the mixing properties of single and multiple confined transverse jets. A new physics-based scaling law variable was developed based on unconfined transverse jet trajectories. This variable accounts for both entrainment and drag momentum transport mechanisms which cause the jet deflection. The utility of this parameter under confined conditions was considered. It was observed that this new scaling parameter does correlate both qualitative and quantitative measures of the mean mixture properties, in particular prior to any jet-wall interactions. It was found that no local optimum mixing condition was present for two and three jets. For six jets, the behavior changed dramatically, with the emergence of a local optimum mixing state that is consistent with previous data collected for gas turbine geometries (Holdeman 1993). It is apparent that the local optimum observed for six jets involves jet penetration to a finite radial position while spreading in the cross plane, leading to the jets blending together resulting in a highly uniform mean mixture fraction distribution. When the number of jets is three or less, this blending process cannot occur due to the excessive distance between the jets. Jet impaction at the pipe center facilitates mixing for two and three jets, while degrading uniformity for six jets.

15. SUBJECT TERMS

16. SECURITY CLASSIFICATION OF:			**17. LIMITATION OF ABSTRACT**	**18. NUMBER OF PAGES**	**19a. NAME OF RESPONSIBLE PERSON**
					Nils Sedano
a. REPORT	**b. ABSTRACT**	**c. THIS PAGE**	SAR	28	**19b. TELEPHONE NO** *(include area code)*
Unclassified	**Unclassified**	**Unclassified**			661-275-5972

Standard Form 298 (Rev. 8-98)
Prescribed by ANSI Std. 239.18

Physics-based Scaling Laws for Confined and Unconfined Transverse Jets

D. J. Forliti[1†], D. V. Salazar[1], and A. J. Bishop[2]

[1]Sierra Lobo, Inc., 10 East Saturn Blvd., Edwards AFB, CA 93524
[2]Air Force Research Laboratory, 10 East Saturn Blvd., Edwards AFB, CA 93524

Abstract

An experimental study was conducted to explore the mixing properties of single and multiple confined transverse jets. A new physics-based scaling law variable was developed based on unconfined transverse jet trajectories. This variable accounts for both entrainment and drag momentum transport mechanisms which cause the jet deflection. The utility of this parameter under confined conditions was considered. It was observed that this new scaling parameter does correlate both qualitative and quantitative measures of the mean mixture properties, in particular prior to any jet-wall interactions. It was found that no local optimum mixing condition was present for two and three jets. For six jets, the behavior changed dramatically, with the emergence of a local optimum mixing state that is consistent with previous data collected for gas turbine geometries (Holdeman 1993). It is apparent that the local optimum observed for six jets involves jet penetration to a finite radial position while spreading in the cross plane, leading to the jets blending together resulting in a highly uniform mean mixture fraction distribution. When the number of jets is three or less, this blending process cannot occur due to the excessive distance between the jets. Jet impaction at the pipe center facilitates mixing for two and three jets, while degrading uniformity for six jets.

1. Introduction

Transverse jets have been studied for several decades due to their relevance to a wide range of flows in nature and engineering (Margason 1993). The unconfined transverse jet, shown in Fig. 1(a) as adopted from Fric and Roshko (1994), has been studied extensively due to the relevance to mixing of effluents under wind/current conditions. This flow field also represents a canonical flow having multiple (and interacting) vortex systems and streamline curvature rendering it a good candidate for model validation studies. The transverse jet also represents a popular platform for exploring vorticity dynamics (Karagozian 1986; Morton and Ibbetson 1996).

The confined transverse jet, on the other hand, is more often associated with engineering applications. Maruyama and colleagues studied the properties of single and dual opposed transverse jets issuing into a circular pipe cross flow (Maruyama et al. 1983; Maruyama et al. 1982; Maruyama et al. 1981). The primary motivation for this work was to provide insight to the chemical engineering community that employs simple configurations such as this to promote chemical and thermal processing. The approach of Maruyama and coworkers was to measure the scalar distribution in the cross plane at various locations downstream of the injection location. The level of uniformity of the mean scalar field is a metric for mixing as achieved by a given geometry and flow condition. It was found through this work that there is an optimum jet to cross flow velocity ratio to achieve the most uniform mean scalar field a few pipe diameters downstream of the injection location. Forney, Nafia, and Vo (1996) investigated the single transverse jet issuing into a pipe flow and also found that the mixture uniformity (when normalized similar to the method of Maruyama) has a local optimum velocity ratio; at much higher velocity ratios, the mixture uniformity becomes monotonically more uniform.

†Corresponding author: david.forliti.ctr@us.af.mil, 661-275-5741.

Confined transverse jets have also been studied in relation to gas turbine combustors. Secondary air is injected and mixed with the hot gas flow generated in the primary combustion zone. The temperature must be highly uniform prior to entering the turbine. The injected air must also help maintain a cool combustor liner, thus one and two jet approaches are generally not acceptable. Holdeman (1993) and coworkers have sustained a multi-decade effort to understand the mixing of multiple confined transverse jets. A very wide design space was considered, including planar, circular, and annular geometries. Holdeman was able to identify an empirical scaling variable that correlates optimum mixing. A parameter C, defined as

$$C = \frac{S}{H}\sqrt{J}\,, \tag{1}$$

where S is the spanwise spacing between jets, H is the characteristic dimension of the cross flow duct, and J is the jet-to-cross flow momentum flux ratio. Holdeman finds that optimum conditions exist when C is equal to approximately 2.5, a condition associated with the jets penetrating approximately half way across the duct. When C is less than 1.25, the jets underpenetrate where the jet fluid stays near the walls, and when C is greater than 5, the jets overpenetrate leading to jet fluid building up near the center of the duct.

Holdeman et al. (1997) summarize an overview of mixing of confined transverse jets when the cross flow is a round pipe. In the context of Eq. 1, the characteristic scale H is equal to the pipe radius R_o, S is defined as the azimuthal spacing between jets at the radial location $R_{1/2}$ that divides the pipe cross section into two equal areas. This radius, $R_{1/2}$ is equal to $R_o/\sqrt{2}$. This allows for a new form for C as

$$C = \frac{\pi\sqrt{2J}}{n}\,, \tag{2}$$

where n is the number of jets. Leong, Samuelsen, and Holdeman (2000) find that this scaling law works for combustion conditions for n ranging from eight to eighteen. Vranos et al. (1991) previously found that the scaling law worked well for six or more jets for a somewhat more complicated geometry that included angled slot jets and a cross flow passage having variable cross-sectional area. Unlike the scaling laws developed for single and two jets issuing into a round pipe (Maruyama, Mizushina and Hayashiguchi 1983), the scaling law shown in Eq. 2 does not depend on the jet diameter. It is clear that these two scaling laws must transition from one to another as the number of jets increases from two to six.

The current work is aimed at exploring the mixing of confined transverse jets, with the objective of developing useful scaling laws in the gap between the flow reactor regime (one or two jets) and the typical gas turbine regime (six or more jets). The study began with an investigation of a physics-based scaling law for the trajectory of unconfined transverse jets. A new scaling variable was developed which demonstrates a good collapse of literature data over a range of conditions. This new scaling law was employed in the study of the mixing of confined

transverse jets and was found to correlate well with both the qualitative nature of the mixture pattern as well as the quantitative mixture uniformity for certain geometries and flow conditions.

2. Scaling the Unconfined Transverse Jet Trajectory

The trajectory of the transverse jet is useful in understanding the mixing and dispersion of jet fluid in an ambient cross flow. It thus represents one of the fundamental characteristics of the transverse jet and is often the target for scaling law development. A number of studies have been conducted to measure and scale the transverse jet trajectory (Cambonie et al. 2013; Cárdenas et al. 2012; Chassaing et al. 1974; Chochua et al. 2000; Fearn and Weston 1974; Gutmark et al. 2008; Hasselbrink and Mungal 2001a; Hasselbrink and Mungal 2001b; Kamotani and Greber 1974; Keffer and Baines 1963; Muppidi and Mahesh 2005; New et al. 2006; Pratte and Baines 1967; Smith and Mungal 1998; Su and Mungal 2004; Yuan and Street 1998). Many of these studies sought to develop a universal trajectory curve with a single or reduced set of independent variables. Several efforts also attempt to account for the shape of the jet velocity profile and/or the properties of the cross-flow boundary layer.

From a fundamental perspective, the jet trajectory will depend on the full set of independent dimensionless groups. Assumptions may be made that when coupled with analysis, suggest that the trajectory depends on a subset of dimensionless groups, ideally a single parameter. For example, Keffer and Baines (1963) argued that the jet deflects due to the relative momentum flux of the jet to the cross flow, resulting in the expectation that the trajectory will scale with r^2D_J, where r is the jet to cross flow velocity ratio and D_J is the jet diameter. The r^2D_J scaling law may also be derived through assuming that the drag force on the jet by the cross flow is the dominant momentum transport mechanism (as will be shown later in this section). They find a good collapse of their trajectory data (which is based on the loci of maximum velocity magnitude) when scaled in this manner, especially when accounting for a near field "virtual origin" effect. Alternatively, Hasselbrink and Mungal (2001a) argue that the entrainment of cross flow fluid with its associated momentum, is the primary momentum transport mechanism. With this assumption and subsequent analysis, Hasselbrink and Mungal find that the jet trajectory scales with rD_J. Hasselbrink and Mungal (2001b) and Smith and Mungal (1998) both find that the trajectory scales reasonably well with rD_J. It should be mentioned that Hasselbrink and Mungal define the jet trajectory as the streamline that originates at the center of the jet in the exit plane, while Smith and Mungal use the loci of maximum jet fluid concentration.

The current authors argue that both the drag force and entrainment play an important role in transporting momentum from the cross flow to the jet. Figure 1(b) shows the control volume that will be used to develop a scaling factor B, such that BD_J represents the transverse length of the control volume. This control volume is defined such that the rate at which momentum is added to the jet in the x direction is equal in magnitude to the rate at which y-momentum is introduced through the jet orifice. Thus BD_J is a length scale associated with momentum transport to the jet, and normalization of the jet trajectory by BD_J is likely to have good collapse. The momentum transport mechanisms are the drag force F_D and the entrainment momentum transport term $M_{entrainment}$. These momentum transport

mechanisms can be estimated using empirical models. The resultant scaling of the trajectory by BD_J is likely to be valid within the limits of applicability of the models used to estimate the two momentum transport terms.

The entrainment term is associated with momentum transported to the jet due to the fact that the cross flow fluid that is entrained by the jet carries with it momentum in the x direction. The entrainment of cross flow into the jet is influenced by the complex aerodynamic interaction between the cross flow and the jet. At a high velocity ratio, the jet would be expected to entrain cross flow fluid nominally as a free jet. A similar argument is employed by Hasselbrink and Mungal (2001a) . Under this approximation, one could use the correlation developed by Ricou and Spalding (1961),

$$\frac{\dot{m}(x)}{\dot{m}_J} = C_e \left(\frac{\rho_J}{\rho_o} \right)^{-1/2} \left(\frac{x}{D_J} \right) , \tag{3}$$

where ρ is density, x is axial position along the jet axis, C_e is the entrainment coefficient, $\dot{m}$ is the jet mass flow rate, and subscripts J and o represent jet and cross flow, respectively. Ricou and Spalding find that the global value for C_e is 0.32 over a range of density ratios at high jet Reynolds numbers (Reynolds number greater than approximately 20000). Hill (1972) and Han and Mungal (2001) both find that the entrainment coefficient is a function of x/D_J that originates near zero (weak entrainment near the orifice) and asymptotes to 0.32 further downstream.

Equation 3 can be used to evaluate the momentum transport to the jet over the distance BD_J, leading to

$$\dot{m}_{entrained} = \dot{m}_J C_e \left(\frac{\rho_o}{\rho_J} \right)^{1/2} B . \tag{4}$$

The momentum transport associated with this entrainment would be

$$\dot{m}_{entrained} U_o = \dot{m}_J C_e \left(\frac{\rho_o}{\rho_J} \right)^{1/2} B U_o , \tag{5}$$

where U_o is the cross flow velocity.

In a similar manner, the drag force on a section of the jet with a streamwise length of BD_J can be estimated using an average drag coefficient. The approximate blockage of the jet to the cross flow is BD_J^2, thus using the definition of the drag coefficient, the drag force may be estimated as

$$F = C_D \rho_o U_o^2 D_J^2 B / 2 , \tag{6}$$

where C_D is the drag coefficient.

Adding the two expressions in Eqns. 5 and 6, setting the sum equal to the initial momentum rate of the jet, one can solve for B as

$$B = \frac{J}{\frac{2C_D}{\pi} + C_e J^{1/2}}. \tag{7}$$

The expression for B encompasses both entrainment and drag effects. If the drag is neglected, B becomes proportional to $J^{1/2}$, leading to BD_J being proportional to rD_J scaling (for uniform density). Neglecting the entrainment mechanism results in BD_J being proportional to r^2D_J scaling. It is interesting to note that the expression B accounts for the density ratio.

Before using the B parameter to attempt scaling jet trajectory data, values for C_e and C_D are required. The value for C_e that is used is the nominal value of 0.32 found in the literature on fully-developed free jets. For the drag coefficient, one might first expect that the jet acts more or less as a cylinder in cross flow. This is clearly true near the jet exit, but the jet experiences deformation that will change the projected area. The analytical study by Mashayek, Jafari, and Ashgriz (2008) on the aerodynamic interactions of a liquid transverse jet issuing into a gaseous cross flow indicates that a nominal representative drag coefficient would be approximately 1.7; this value will be used in the present study.

Before presenting the trajectory scaling using BD_J, we first present literature data scaled using rD_J and r^2D_J. Data from literature is limited to moderately high jet Reynolds numbers, nominally greater than 5000, and thin cross flow boundary layers, approximately $\delta/D_J < 0.25$. Data is also limited to velocity ratios greater than approximately four. Lower velocity ratio transverse jets are likely to have entrainment characteristics that are significantly different than a free jet. Figure 2 shows the velocity maxima trajectory for a number of cases from literature scaled with rD_J and r^2D_J (Chassaing, George, Claria and Sananes 1974; Chochua, Shyy, Thakur, Brankovic, Lienau, Porter and Lischinsky 2000; Fearn and Weston 1974; Kamotani and Greber 1972; Keffer and Baines 1963; Su and Mungal 2004). As can be seen from the figures, these scaling laws have a significant level of scatter. Figure 3 shows BD_J scaling for the same cases as shown in Fig. 2, and it is very clear that the BD_J normalization provide a very good correlation of the data. The Su and Mungal data, which is for their elevated jet case, is somewhat different, although it should be mentioned that they defined the trajectory as the loci of maximum velocity with the cross flow velocity subtracted, thus it is expected this trajectory would be slightly different. The curve fit of the data (not including the Su and Mungal data) has the form

$$\frac{y}{BD_J} = 0.0026\left(\ln\left(\frac{x}{BD_J}\right)\right)^3 + 0.0485\left(\ln\left(\frac{x}{BD_J}\right)\right)^2 + 0.332\left(\ln\left(\frac{x}{BD_J}\right)\right) + 0.9854. \tag{8}$$

It should be pointed out that most of the data included in this figure is limited to axial distances less than approximately 20 jet diameters. The good collapse of the data is somewhat surprising in light of the findings of Hill (1972) and Han and Mungal (2001) that the entrainment is weaker in the near field of a free jet. Hill found that the entrainment coefficient reaches the nominal value of 0.32 around x/D_J of 10. Thus much of the data in Fig. 3 would be in the degraded entrainment range if the transverse jet follows the free jet trend. There are a couple of possible explanations for why the value of 0.32 seems to work well. First, the presence of the cross flow may alter the development of structure in the jet shear layer, and this may result in an acceleration of the entrainment maturation process. Secondly, it is also expected that once the transverse jet matures and develops a counter-rotating vortex pair, the entrainment is expected to be higher than that of a free jet (Yuan and Street 1998). Thus the 0.32 value may be a reasonable average value over the spatial range of the data. Further investigation will be required to explore these possibilities. It is apparent that using the two values for C_e and C_D accounts for the relative contribution of these two momentum transport mechanisms. It should also be mentioned that the form of B given in Eq. 7 may be valid for other jet shapes, and the two coefficients may be used as free parameters to obtain collapse of multiple profiles. This should be effective as long as there are representative average values for C_e and C_D for a given jet shape.

It must be emphasized that the collapse of the trajectory data shown in Fig. 3 is not universal, as only a subset of literature data has been used. Data shown in Fig. 3 is limited to thin relative cross flow boundary layers, velocity ratios above approximately four, and jet Reynolds numbers above approximately 5000. Cases in the literature outside these conditions demonstrate deviations when scaled with BD_J. The deviation is likely due to a variety of sources. As the velocity ratio decreases below approximately four, the likelihood of jet-like entrainment decreases as the cross flow is able to more readily disturb the jet structure. When the boundary layer is thick (of the order of the jet diameter D_J), the jet passes through a region of lower momentum cross flow before reaching the freestream. This will effectively degrade the drag force near the jet exit. Low Reynolds number transverse jets also exhibit much more laminar structure (New, Lim and Luo 2006) that will diverge from the fully-turbulent entrainment law. Nonetheless, Fig. 3 highlights the importance of considering drag and momentum as important factors, at least in the range of conditions considered.

As an alternative to the local velocity maxima trajectory, the streamline originating from the center of the jet is often used to characterize the jet trajectory. Figure 4 shows some data from literature using this definition of the jet trajectory. Included in the figure is the curve fit from Fig. 3, and both velocity and streamline data for a velocity ratio r = 3.3 from Yuan and Street (1998). The velocity-based trajectory matches well the scaling law from Fig. 3, even though the velocity ratio is below four. The two Hasselbrink and Mungal (2001b) trajectories collapse well on one another, but do not overlap with the curve from Fig. 3 or other data shown in Fig. 4. Intuitively, one might expect the streamline to exhibit more scatter and sensitivity to the jet near field, due to the fact that it is a spatially-integrated characteristic. The work of Yuan and Street (1998) supports this view, as they find that the streamline trajectory is more sensitive to buoyancy effects in comparison to the maximum velocity trajectory.

Figure 5 shows the third most common trajectory that is based on the loci of maximum mean scalar concentration. Beginning with the work of Smith and Mungal (1998), the collapse of the trajectories for velocity ratios above ten is good. The collapse is improved compared to the rD_J and r^2D_J scaling presented by Smith and Mungal. Also shown in the figure are the trajectories from Su and Mungal (2004) and Yuan and Street (1998). Both of these studies considered jets issuing from fully-developed pipe flow. The Yuan and Street simulations are in agreement with the high velocity ratio data of Smith and Mungal, while the Su and Mungal data demonstrates significantly greater penetration. The Su and Mungal case has been favorably compared to direct numerical simulation data of Muppidi and Mahesh (Muppidi and Mahesh 2005; Muppidi and Mahesh 2008), with both experiment and simulation showing a relatively long jet core extending into the cross flow. The difference between the Yuan and Street and Su and Mungal is likely due to initial conditions. The Su and Mungal jet Reynolds number being 5000, the initial conditions are fully-developed and turbulent. The turbulence in the initial conditions disturbs the initial jet boundary where the shear layer is seen to be spreading relatively weakly. The exit turbulence appears to be interfering with the early shear layer development. The conditions of Yuan and Street, on the other hand, are at a lower Reynolds number, and the shear layer instability appears to develop very quickly.

In summary, a parameter B has been developed that accounts for momentum transport due to entrainment and drag. Scaling the jet trajectory, in particular the maximum velocity trajectory, using BD_J appears to generate a single curve as long as a set of variable constraints are satisfied. The question arises as to whether a parameter such a B has utility under confined conditions. The expression BD_J is a jet trajectory length scale. Assuming the jet issues into a pipe of diameter D_o, one might expect that the ratio of these length scales, referred to as K, where

$$K = \frac{BD_J}{D_o}, \tag{9}$$

may be a candidate parameter for confined transverse jets. The present experimental effort explores the utility of K as a parameter to characterize the mixing of confined transverse jets.

3. Experimental Facility

The experimental facility is shown in Fig. 6. Demineralized water is used as the working fluid for both the main flow and the jets. The main flow is driven using an Ebara A3U32-200 pump. A hand valve is used to control the flow rate to the experiment, which is measured using a Flow Technology Inc. model FT-16A50-LB turbine flow meter. Excess water is recirculated back to the main flow supply tank. The jet fluid consists of demineralized water mixed with a trace concentration of sodium fluorescein, a fluorescent agent used to discriminate jet and main flow fluid. High-pressure nitrogen is regulated and delivered to the jet fluid tanks to drive the flow. A control valve and rotameter are used to control and meter the overall jet flow rate. The test section consists of a manifold of the jet flow to up to six azimuthally-spaced jets. Each jet has a ball valve to allow for zero, one, two, three, and six jet configurations. Interchangeable jet insert components allow for different jet diameters to be installed.

A schematic of the test section is shown in Fig. 7. The inner diameter of the main flow D_o is 4.04 cm. Several diameters of length (greater than 20) between the test section and control valve allow the flow to achieve a fully-developed turbulent state. The main flow Reynolds number is maintained above 6000. Planar laser-induced fluorescence (PLIF) was used to measure the cross plane concentration of jet fluid at an axial distance $3D_o$ downstream of the injection location. Jet numbers of one, two, three, and six were considered, maintaining azimuthal symmetry for multiple jet cases. Table 1 shows a summary of parameter ranges for the current study. The parameter K was the primary flow parameter considered in the study.

Parameter	Range
n	1, 2, 3, 6
J	1.8-50
Re_j	> 6000
Re_o	> 6000
D_j/D_o	0.12, 0.165, 0.21
K	0.25-1.75

Table 1: Summary of operating conditions

A schematic of the PLIF optical setup is shown in Fig. 8. The concentration of sodium fluorescein in the jet fluid supply tanks was varied depending on the relative experimental flow rates to maintain test section concentrations below approximately 3×10^{-7} mol/L, which in the context of the size of the test section, minimizes laser absorption (Walker 1987). Sodium fluorescein absorbs and emits in a band centered on 490 and 519 nm, respectively. The fluorescence is induced using the 488 nm line of a 225 mW National Laser model 800AL argon-ion laser. The 488 nm line is isolated from the multiline laser output using an Edmund Optics dichroic mirror. A phantom V7.1 CMOS camera is used to capture PLIF images. A Thorlabs long pass optical filter is placed between the camera and the light sheet to remove the 488 nm from the fluorescence signal. The camera and fluorescence were independently verified as being linear in the rage used for the experiments.

A set of calibration images was collected throughout each test day with known mixture fractions. For the calibration pictures, the jet fluid is injected far upstream (approximately 50 pipe diameters) of the test section to ensure fully mixed flow at the measurement location. The mixture fraction for each pixel in the experimental images is calculated using a curve fit from the calibration images. This calibration approach allows for correction of light sheet intensity variations. The presence of small particles that collect on the test section walls and/or optical components leads to some transients in the light sheet intensity structure, resulting in some streaks being present in the data.

Laser Doppler velocimetry was used to characterize the main flow initial conditions. A miniLDV system from Measurement Sciences Inc. was used to measure the velocity profile in the main pipe. Figure 9 shows a representative radial profile of the mean and rms fluctuation velocities. Data from van Doorne and Westerweel

(2007) are shown for comparison. The velocity profiles of the transverse jets were not measured due to the small scale and lack of adequate optical access. The jet insert elements had a minimum length of 20 jet diameters to allow the flow to become fully developed. Based the results of Ajayi, Papadopoulos and Durst (1998), this should be a sufficient distance to produce fully-developed turbulent flow characteristics at the jet exit. A variety of flow conditioning elements were tested in the jet inserts with no noticeable changes in the resultant mixing characteristics as measured at $x/D_o = 3$.

4. Results

Results will first be presented for a single transverse jet. Figure 10 shows examples of the instantaneous and mean mixture fraction distributions for $K = 1.25$ and $D_J/D_o = 0.165$. For this test, the jet is located at 90° clockwise from the vertical coordinate. Bright regions in the figure represent higher relative concentration of jet fluid. For this operating condition, the mixture fraction is higher on the opposite side of the pipe relative to the injection location, suggesting the jet flow has penetrated across the pipe and has impacted the opposite wall. In general, the instantaneous distribution can deviate significantly from the mean distribution, suggesting the presence of large-scale unsteady motion.

Emphasis was placed on characterizing the mean mixture distributions, thus resolution of the smallest scales in the flow field was not considered a requirement. Each mean image was based on 200 instantaneous images, with each instantaneous image having an exposure time of 50 ms. The images were collected at a rate of 10 Hz, thus the mean represents a time average over ten seconds. Repeatability tests demonstrated that the sampling time was sufficiently long to average out any low-frequency phenomena. Local mean mixture fraction measurements were in general repeatable within about 0.05, with the area-weighted average within a few percent.

Figure 11 shows the mean mixture fraction distributions for the single jet for a variety of flow conditions and diameter ratios. Across each row, K varies from 0.25 to 1.75 in 0.25 increments, starting from left to right. Each row represents a different diameter ratio, ranging from 0.12 for Fig. 11(a) to 0.21 for Fig. 11(c). Once again, the jet is injected at 90° clockwise from the vertical axis. For the top row, with K increasing from left to right, the location of the jet moves across the pipe as expected. For K near unity, the jet fluid spreading appears to begin to be governed by the constraints induced by the pipe wall. Once the jet begins to interact with the wall, the jet fluid deflects along the pipe wall, eventually returning back to the location where injection occurs. For this jet size, the jet fluid can even be re-entrained towards the middle as shown for the $K = 1.75$ case.

The utility of parameter K as an indicator of flow regime is illustrated in the figure. Each vertical row, representing a constant value of K, shows strong similarity for the different diameter ratios. This is particularly the case before a strong interaction occurs with the wall, that is, for $K \leq 1$. The strong similarity for the different diameter ratios for $K < 1$ suggests the trajectories are likely very similar; the trajectories of confined transverse jets are not measureable with the current facility but will be considered in future efforts with a different facility. For $K > 1$, the smallest diameter ratio shows a more complex variation with K than the larger diameter ratios. Thus in the jet/wall

interaction regime, the qualitative distribution of the mean mixture fraction depends on K and the diameter ratio D_J/D_o.

The "unmixedness" of the distribution, which is often an important figure of merit for a mixing device, may be quantified using a variety of definitions. The most common measure of variation of the mean mixture ratio distribution involves either the variance or standard deviation of the spatial samples. This variation should be normalized to allow relative comparison between different geometries and flow conditions. The most common choice for normalization is an estimate of the variation (either variance or standard deviation) near the injection location. Thus this normalization represents the measured spatial variation relative to the worst case scenario. In the present study, the unmixedness U will be defined as

$$U = \frac{\sigma_z}{\sqrt{\bar{z}(1-\bar{z})}}, \tag{10}$$

where σ_z is the measured standard deviation of the mean mixture fraction field z, and $\bar{z}$ represents the expected mean mixture fraction based on the relative flow rates (which may differ slightly from the area-weighted mean of z). This definition for U is the square root of the unmixedness used by Bain, Smith, and Holdeman (1995). Note that (1-U) would be a good definition for mixing device efficiency.

Figure 12 shows the unmixedness U for the single confined transverse jet scaled against a variety of flow parameters including the K, J, and β which is the momentum ratio,

$$\beta = Jn\frac{D_J^2}{D_o^2}. \tag{11}$$

Figure 12(a) shows the unmixedness as a function of K for different diameter ratios. The curves are very similar in shape, and demonstrate the expected local optimum point observed by Maruyama and coworkers (Maruyama, Mizushina and Hayashiguchi 1983; Maruyama, Mizushina and Watanabe 1982; Maruyama, Suzuki and Mizushina 1981). The local optimum points are aligned and are associated with K = 0.75. Note that this optimum point may depend on the measurement location, which is this study is fixed at $x/D_o = 3$. In general, the unmixedness reduces with decreasing diameter ratio. In the impaction regime, associated with K > 1, the curves are similar in shape and nominally parallel to one another. Initially impaction (K ~ 1) degrades uniformity, but once K increases above 1.25, impaction facilitates mixing. There are two potential aspects that may influence the role impaction plays on the mixing process. The first is the relative intensity of the impaction, and the second is the position of the impaction relative to the measurement location. The relative intensity of the impaction appears to depend on a flow parameter like K or β. Strong impaction may appear to impede mixing in the impaction near field, but may result in good mixing further downstream. This would likely lead to an optimum K which depends on measurement location. This aspect will be explored in future studies.

Figures 12(b) and (c) show the unmixedness U plotted against J and β. As expected, neither parameter provides as good a correlation compared to K, although it appears that in the impaction regime, J provides some collapse. Higher J values for the larger two jet sizes would be required to investigate this. Overall, Figures 11 and 12 suggest that the parameter K performs well in correlating the qualitative and quantitative mixture fraction characteristics, particularly prior to jet impaction on the wall.

Figure 13 shows the optimum velocity ratio as a function of diameter ratio. Data from literature and the current study are included (Cozewith and Busko Jr 1989; Forney, Nafia and Vo 1996; Maruyama, Mizushina and Hayashiguchi 1983; Maruyama, Mizushina and Watanabe 1982; Maruyama, Suzuki and Mizushina 1981). In general, the current data is in strong quantitative agreement with the work of Maruyama. Curves of constant K are shown in the figure. The curve for K = 0.75 goes through the current data and some of the Maruyama data, whereas K = 1.0 seems to provide a better overall agreement with all of the data. It should be mentioned that the Cozewith and Busko (1989) data is based on chemical reactions, thus is biased toward fine scale mixing which is required to facilitate chemical reaction. The work of Forney, Nafia, and Vo (1996) is based on RANS calculations.

A configuration having two opposing transverse jets issuing into a pipe has been explored in a limited manner in the literature. Maruyama, Mizushina, and Hayashiguchi (1983) found that the optimum velocity ratio for two opposed jets followed the same trend as the single jet (this data is included in Fig. 13). The two jet configuration was investigated in the current study to gain further insight on the utility of the K parameter. Figure 14 shows the mean distribution for the two jet configurations, using the same diameter ratios and range of K as was done for the single jet in Fig. 11. Once again, vertical columns represent fixed K values for the three different diameter ratios. The jets were located at 90° and 270°. At K = 0.25, the jets can be seen to penetrate to a similar depth as for the single jet case, although the jets begin to blend together. As K increases through values of 0.5 and 0.75, the jets experience a collision at the main pipe center, and jet fluid deflects back towards to the pipe walls in the other plane. This off-axis splitting of the jets was also observed by Maruyama et al (1983). Through these three K values, the qualitative behavior is very similar for a constant value of K. As K increases to unity, the deflected jet fluid reaches and interacts with the pipe wall. At the higher K values, the jet fluid is preferentially located on the top and bottom of the pipe, due to the deflection of the jets after the collision and the subsequent interaction with the wall.

The unmixedness of the dual jet configurations is shown in Fig. 15. It appears that all three diameter ratios are void of a local optimum point. The study of Maruyama et al. (1983) show that the local optimum only emerges downstream. Although we observe no local optimum at $x/D_o = 3$, one may emerge further downstream. Overall, Fig. 15 demonstrates that the parameter K provides the best collapse of the data. Compared to the unmixedness for a single jet (Fig. 12), the two jet configuration generates a higher level of uniformity.

The mean mixture fraction distributions for the three jet configurations are shown in Fig. 16. In these cases, the activated jets are at 30°, 120°, and 270°. For $K \leq 0.75$, the different diameter ratio cases undergo a similar evolution including penetration into the pipe flow, followed by a collision process at the center, and ejection of jet fluid back

towards the pipe wall at the locations between the jets (i.e. at 90°, 210°, and 330°). The qualitative behavior scales well with K for the different diameter ratios. For $K \geq 1$, the jet fluid experiences an interaction with the pipe wall. For the smallest jet, the distribution quickly achieved a nearly axisymmetric distribution with slightly higher jet fluid concentration at the center of the pipe. For the middle size jet, the transition from the triangular like pattern at K = 0.75 and the axisymmetric centered pattern is much more gradual, occurring over a range of K from 1.0 to 1.75. The evolution of the largest jet configuration shows further slowing of the transition, and does not achieve the near axisymmetric nature within the range of conditions considered. Once again, the qualitative flow regime depends on K and D_J/Do in the wall interaction regime.

The unmixedness trends shown in Fig. 17 provide further evidence towards the utility of the K parameter as a scaling variable. As expected, in the pre-wall interaction regime ($K < 1$), the unmixedness collapses relatively well for all diameter ratios, while some scatter is present in the wall interaction regime ($K \geq 1$). The momentum ratio β shown in Fig. 17(c) shows some promise as a scaling parameter for β greater than about unity. This collapse is likely just fortuitous as nominally constant β values for the different jet sizes have qualitatively very different distributions.

The mean mixture fraction distributions for the six jet configuration is shown in Fig. 18. Only the small and large diameter ratio geometries were considered for six jets. For the small jet case shown in Fig. 18(a), the jets penetrate into the pipe flow, achieve a highly uniform state at K = 0.5, and quickly transitions to the nearly axisymmetric state that was seen for the three jet configurations. The same qualitative behavior is demonstrated for the large diameter ratio case as shown in Fig. 18(b), although once again the progression with increasing K appears to be slower. It is apparent that the six jet case does not exhibit the strong correlation with constant K, except for K = 0.25.

The unmixedness trends shown in Fig. 19 highlight the different behavior for the six jet configurations. Both diameter ratios show a relatively strong local optimum, although the sharpness of the local optimum is stronger for the smaller diameter ratio. The local optima are no longer at constant values of K, suggesting that the six jet behavior has crossed over into a new regime of behavior compared to the other configurations. The unmixedness as a function of J shows a better correlation in that the local optima appear at a constant momentum flux ratio of approximately eight. This is more consistent with the Holdeman scaling law, Eq. 2, which shows for a fixed C value representing optimum conditions, the momentum flux ratio depends only on the number of jets and does not depend on the diameter ratio. Indeed, the C value for the optimum six jet cases is 2.1, which is generally within the range recommended by Holdeman for optimum mixing (Holdeman 1993; Holdeman, Liscinsky, Oechsle, Samuelsen and Smith 1997). The present data asserts that the six jet configuration is different than all of the other configurations tested during the present study, and that Holdeman scaling works well for six jets. It should be mentioned that operating in an overpenetration regime ($J >> 8$) results in highly degraded uniformity, especially for the smaller diameter ratio. The Holdeman mechanism is highly localized, requiring a single design point to be maintained.

It is very clear that the mixing properties for six (and more) jets is very different from one to three. This is illustrated in Fig. 20 for three and six jets. In the case of three jets, with increasing K (or J), the jets are brought together at the center of the pipe where a strong collisional type interaction occurs. The collision eventually leads to jet fluid being ejected back towards the pipe wall. Eventually at sufficiently high K, the jet fluid will be preferentially concentrated at the center of the pipe with a nearly axisymmetric distribution. The jet-jet and jet-wall interactions in general contribute to the mixing process, at least for the present axial measurement location. For six jets, it appears that the jets experience a different type of interaction that leads to a very uniform local optimum point. As J (or K) increases from a low value, the jets penetrate further into the pipe, and eventually spread in the azimuthal direction at a finite radius where the jets blend together. The jets have diffused in the cross plane to sufficiently fill the cross section, resulting in a highly-uniform state. This condition is well-predicted using the Holdeman correlation. As J increases from this local optimum, the uniformity degrades, resulting in jet fluid biased towards the center of the pipe. This state appears to be sustained as J is increased further. The Holdeman optimum appears to be more of a global, not local, optimal state.

5. Conclusions

The current study explored physics-based scaling laws for the mixing properties of single and multiple confined transverse jets. A scaling law variable, which is based on an analysis of momentum transport to the jet through entrainment and drag, was found to correlate trajectories for a large section of the transverse jet literature data space. This variable was used to define a confined transverse jet parameter K, which was found to have good correlating properties for confined jets, especially before the jet flow interacts with the pipe walls. Once the jet flow hits the pipe wall, the behavior appears to be dependent on multiple parameters, for instance K and the jet-to-pipe diameter ratio. For two and three jets, the unmixedness monotonically decreased with increasing K, at least at three main pipe diameters downstream of the injection location. The six jet configurations demonstrated a different dependence, and did not correlate well with K. In contrast to the two and three jet cases, the six jet configuration resulted in decreased mixing with an increase in J (or K) once the local optimum is surpassed. The optimum mixing state for the six jet cases correlated well with the Holdeman parameter, which was developed over a broad set of experiments and calculations for multiple confined transverse jets. In this regime, the jets will reach a certain radial location, where they have spread to sufficient size in the cross section, to achieve a highly well-mixed state. It is apparent that when fewer jets are used, they cannot blend together at this radial location, and only interact when they have sufficient momentum to impact at the pipe center.

6. References

Ajayi K, Papadopoulos G, Durst F (1998) Influence of upstream development on the losses incurred by flow past an axisymmetric sudden contraction Proc 36th Aerospace Sciences Meeting and Exhibit, AIAA-98-0794, Reno, USA.

Bain D, Smith C, Holdeman J (1995) Mixing analysis of axially opposed rows of jets injected into confined crossflow. J Pow Prop 11:885-893

Cambonie T, Gautier N, Aider J-L (2013) Experimental study of counter-rotating vortex pair trajectories induced by a round jet in cross-flow at low velocity ratios. Exp Fluids 54:1-13

Cárdenas C, Denev JA, Suntz R, Bockhorn H (2012) Study of parameters and entrainment of a jet in cross-flow arrangement with transition at two low Reynolds numbers. Exp Fluids 53:965-987
Chassaing P, George J, Claria A, Sananes F (1974) Physical characteristics of subsonic jets in a cross-stream. J Fluid Mech 62:41-64
Chochua G, Shyy W, Thakur S, et al. (2000) A computational and experimental investigation of turbulent jet and crossflow interaction. Numerical Heat Transfer: Part A: Applications 38:557-572
Cozewith C, Busko Jr M (1989) Design correlations for mixing tees. Industrial & Engineering Chemistry Research 28:1521-1530
Fearn R, Weston RP (1974) Vorticity associated with a jet in a cross flow. AIAA J 12:1666-1671
Forney L, Nafia N, Vo H (1996) Optimum jet mixing in a tubular reactor. AIChE Journal 42:3113-3122
Fric T, Roshko A (1994) Vortical structure in the wake of a transverse jet. J Fluid Mech 279:1-47
Gutmark E, Ibrahim I, Murugappan S (2008) Circular and noncircular subsonic jets in cross flow. Phys Fluids 20:5110-5126
Han D, Mungal M (2001) Direct measurement of entrainment in reacting/nonreacting turbulent jets. Comb Flame 124:370-386
Hasselbrink E, Mungal M (2001a) Transverse jets and jet flames. Part 1. Scaling laws for strong transverse jets. J Fluid Mech 443:1-25
Hasselbrink E, Mungal M (2001b) Transverse jets and jet flames. Part 2. Velocity and OH field imaging. J Fluid Mech 443:27-68
Hill B (1972) Measurement of local entrainment rate in the initial region of axisymmetric turbulent air jets. J Fluid Mech 51:773-779
Holdeman J (1993) Mixing of multiple jets with a confined subsonic crossflow. Progress in Energy and Combustion Science 19:31-70
Holdeman J, Liscinsky D, Oechsle V, Samuelsen G, Smith C (1997) Mixing of Multiple Jets With a Confined Subsonic Crossflow: Part I—Cylindrical Duct. ASME J Eng Gas Turb Pow 119:852
Kamotani Y, Greber I (1972) Experiments on a turbulent jet in a cross flow. AIAA J 10:1425-1429
Kamotani Y, Greber I (1974) Experiments on confined turbulent jets in cross flow. NASA CR-2392
Karagozian A (1986) An analytical model for the vorticity associated with a transverse jet. AIAA J 24:429-436
Keffer J, Baines W (1963) The round turbulent jet in a cross-wind. J Fluid Mech 15:481-496
Leong M, Samuelsen G, Holdeman J (2000) Optimization of jet mixing into rich, reacting crossflow. J Pow Prop 16:729-735
Margason R (1993) Fifty years of jet in cross flow research AGARD Computational and Experimental Assessment of Jets in Cross Flow.
Maruyama T, Mizushina T, Hayashiguchi S (1983) Optimum conditions for jet mixing in turbulent pipe flow. International Chemical Engineering 23:707-716
Maruyama T, Mizushina T, Watanabe F (1982) Turbulent mixing of two fluid streams at an oblique branch. International Chemical Engineering 22:287-294
Maruyama T, Suzuki S, Mizushina T (1981) Pipeline mixing between two fluid streams meeting at a T-junction. International Chemical Engineering 21:205-212
Mashayek A, Jafari A, Ashgriz N (2008) Improved model for the penetration of liquid jets in subsonic crossflows. AIAA J 46:2674-2686
Morton BR, Ibbetson A (1996) Jets deflected in a crossflow. Exp Therm Fluid Sci 12:112-133
Muppidi S, Mahesh K (2005) Study of trajectories of jets in crossflow using direct numerical simulations. J Fluid Mech 530:81-100
Muppidi S, Mahesh K (2008) Direct numerical simulation of passive scalar transport in transverse jets. J Fluid Mech 598:335-360
New T, Lim T, Luo S (2006) Effects of jet velocity profiles on a round jet in cross-flow. Exp Fluids 40:859-875
Pratte B, Baines D (1967) Profiles of the round turbulent jet in a cross flow. J Hydronaut Div ASCE 92:53-64
Ricou F, Spalding D (1961) Measurements of entrainment by axisymmetrical turbulent jets. J Fluid Mech 11:21-32
Smith S, Mungal M (1998) Mixing, structure and scaling of the jet in crossflow. J Fluid Mech 357:83-122
Su L, Mungal M (2004) Simultaneous measurements of scalar and velocity field evolution in turbulent crossflowing jets. J Fluid Mech 513:1-45
Van Doorne C, Westerweel J (2007) Measurement of laminar, transitional and turbulent pipe flow using stereoscopic-PIV. Exp Fluids 42:259-279

Vranos A, Liscinsky D, True B, Holdeman J (1991) Experimental study of cross-stream mixing in a cylindrical duct 27th Joint AIAA, SAE, ASME, and ASEE Propulsion Conference. Sacramento, CA,
Walker D (1987) A fluorescence technique for measurement of concentration in mixing liquids. Journal of Physics E: Scientific Instruments 20:217
Yuan L, Street R (1998) Trajectory and entrainment of a round jet in crossflow. Phys Fluids 10:2323-2335

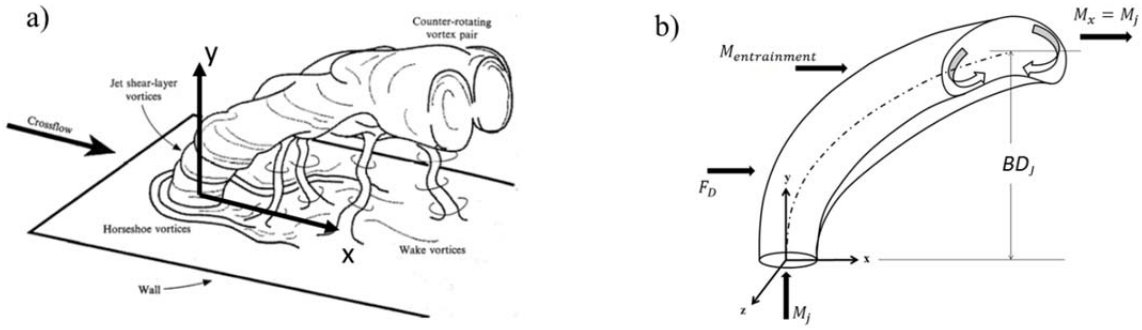

Figure 1: a)Schematic (adopted from Fric and Roshko) and b) control volume of the transverse jet.

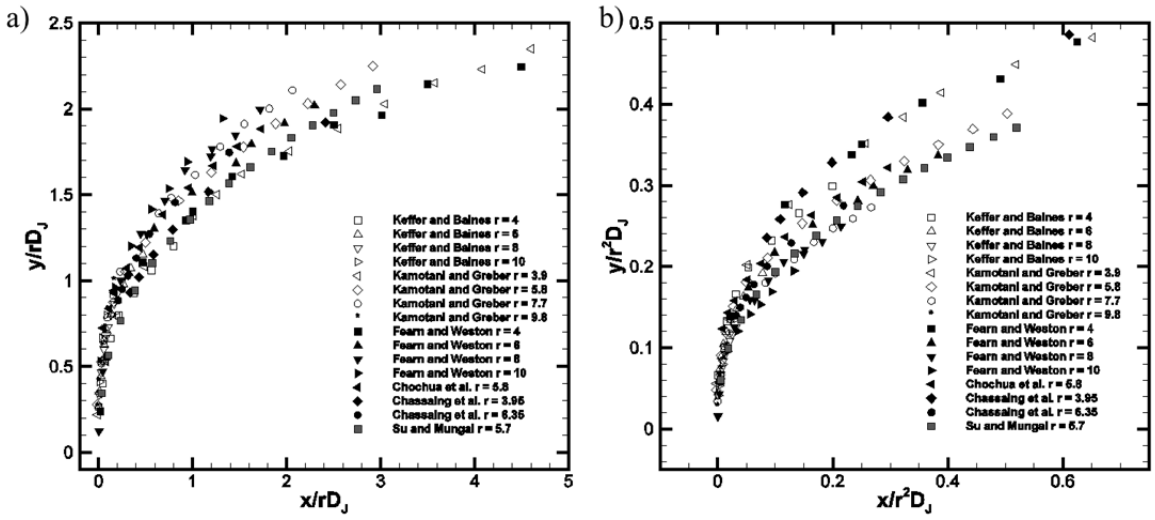

Figure 2: Unconfined transverse jet trajectories scaled with a) rD_J and b) r^2/D_J.

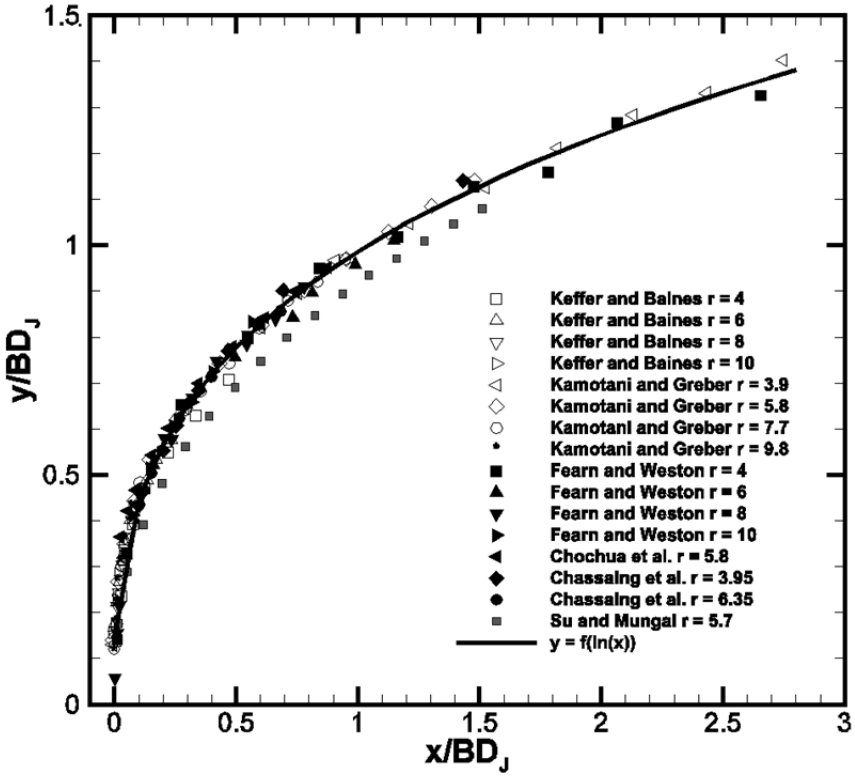

Figure 3: Unconfined transverse jet trajectories scaled with BD_J.

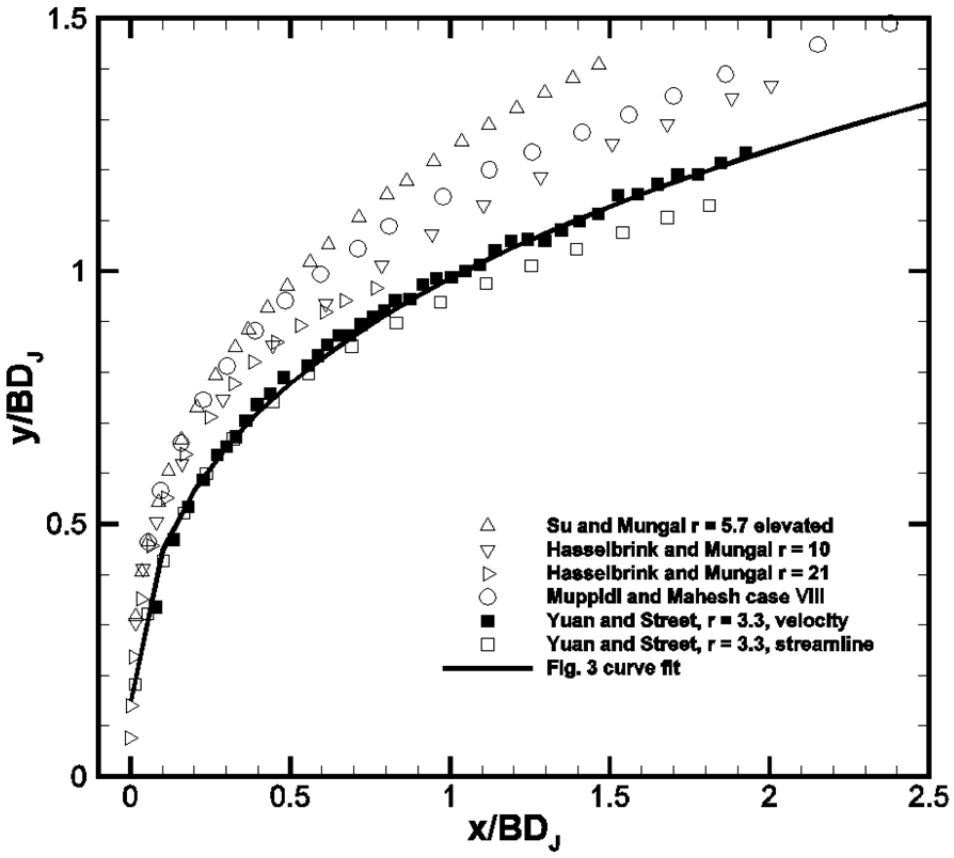

Figure 4: Center streamline unconfined transverse jet trajectories scaled with BD_J.

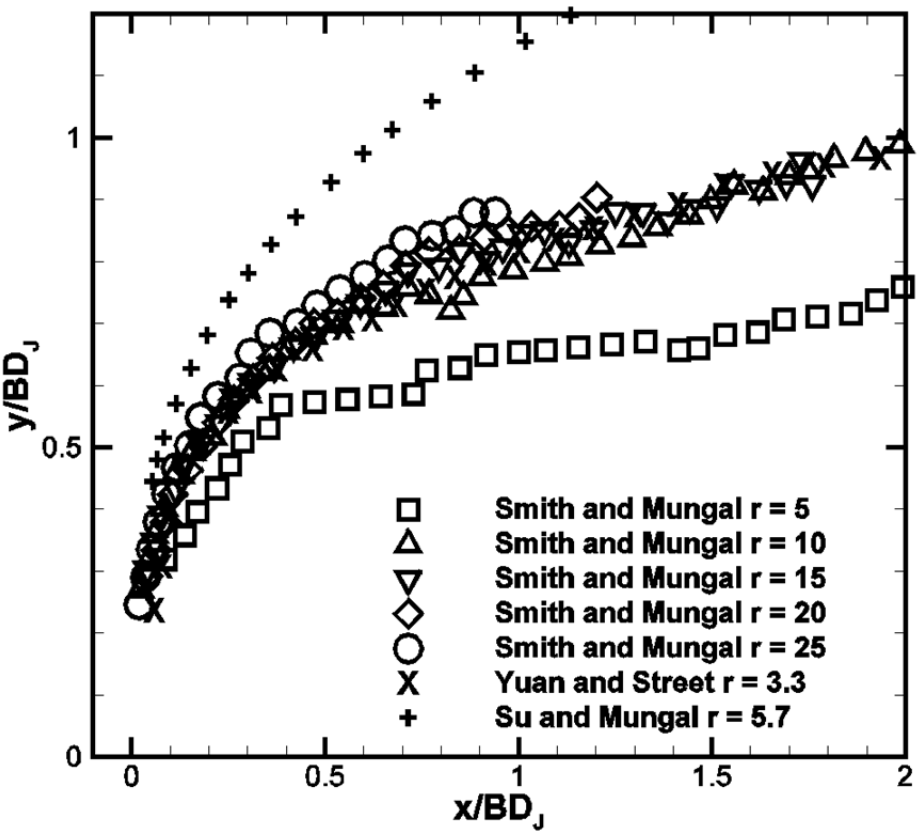

Figure 5: Scalar-based unconfined transverse jet trajectories scaled with BD_J.

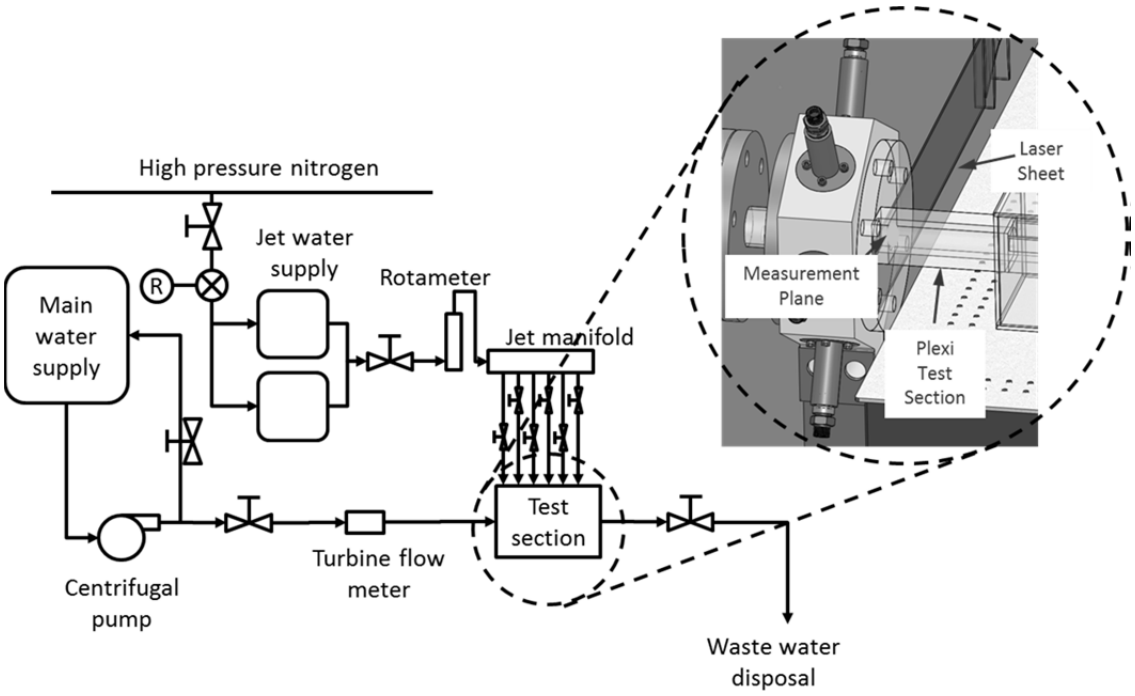

Figure 6: Layout of the experimental facility.

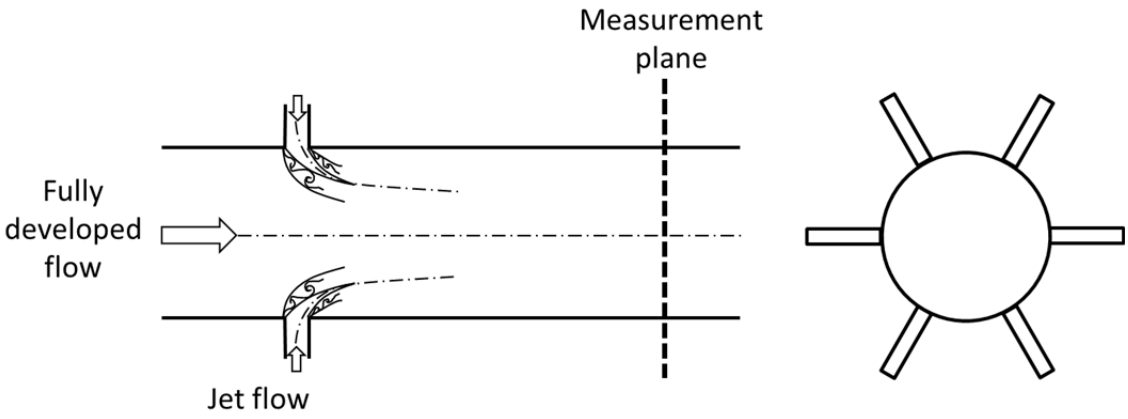

Figure 7: Schematic of the confined transverse jet experiment.

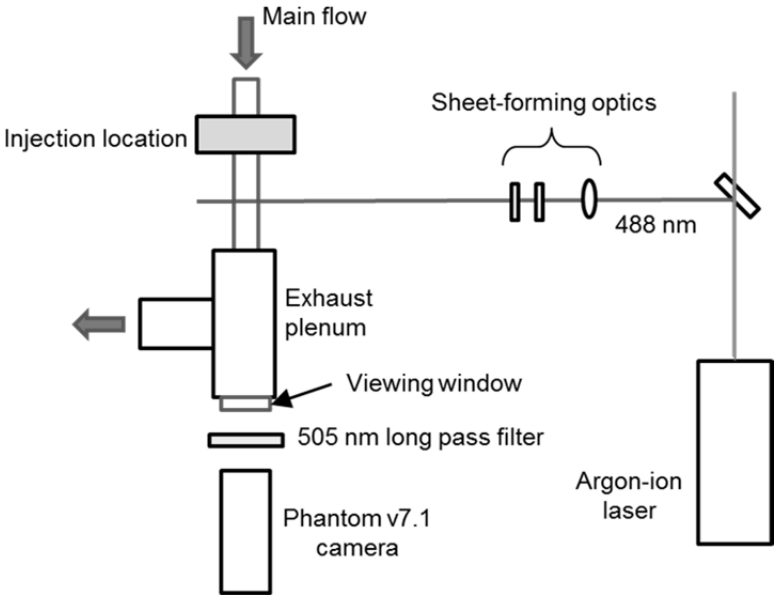

Figure 8: Schematic of the planar laser-induced fluorescence setup.

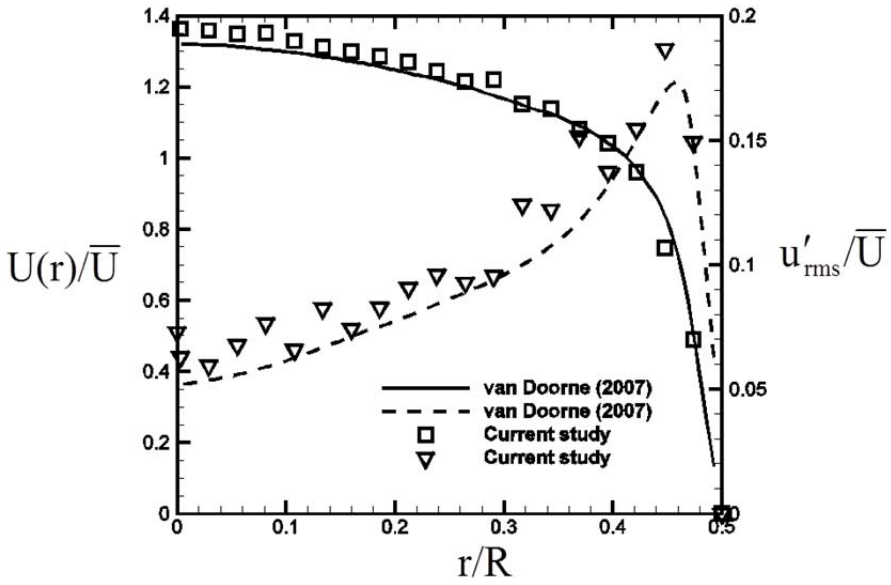

Figure 9: Representative initial conditions of the main pipe flow.

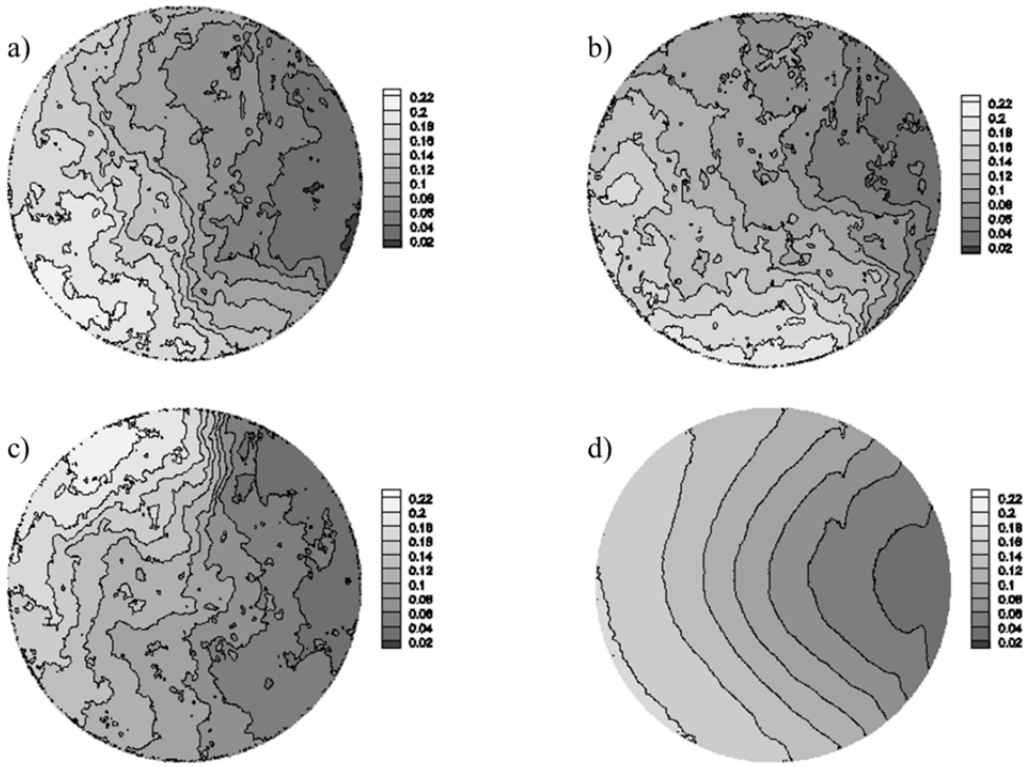

Figure 10: Representative distributions of a-c) instantaneous and d) mean mixture fraction distribution.

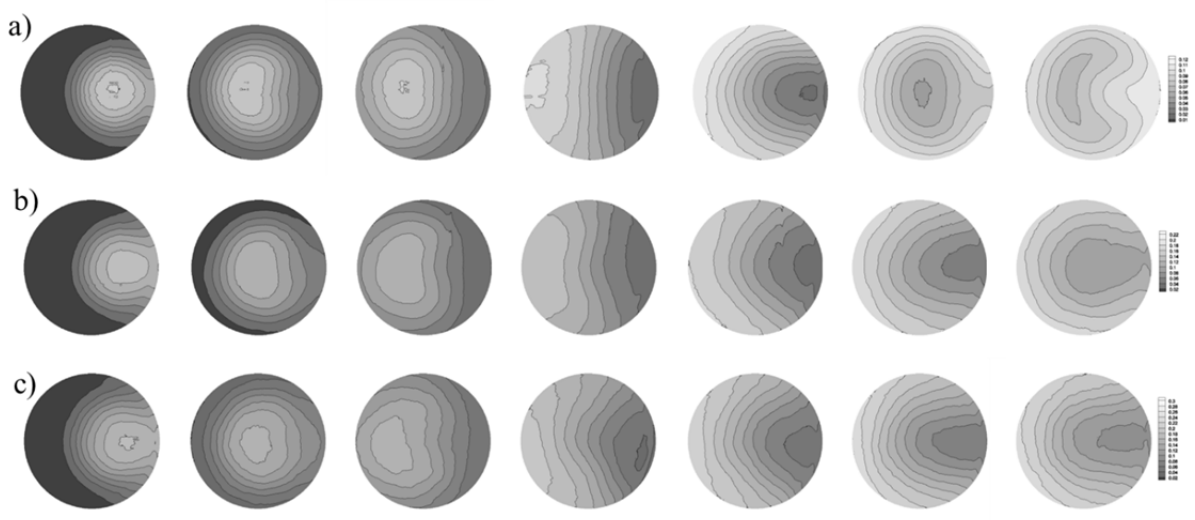

Figure 11: Mean mixture fraction distribution for a single transverse jet for D_J/D_o = a) 0.12, b) 0.165, and c) 0.21, with K increasing from left to right from 0.25 to 1.75 in increments of 0.25.

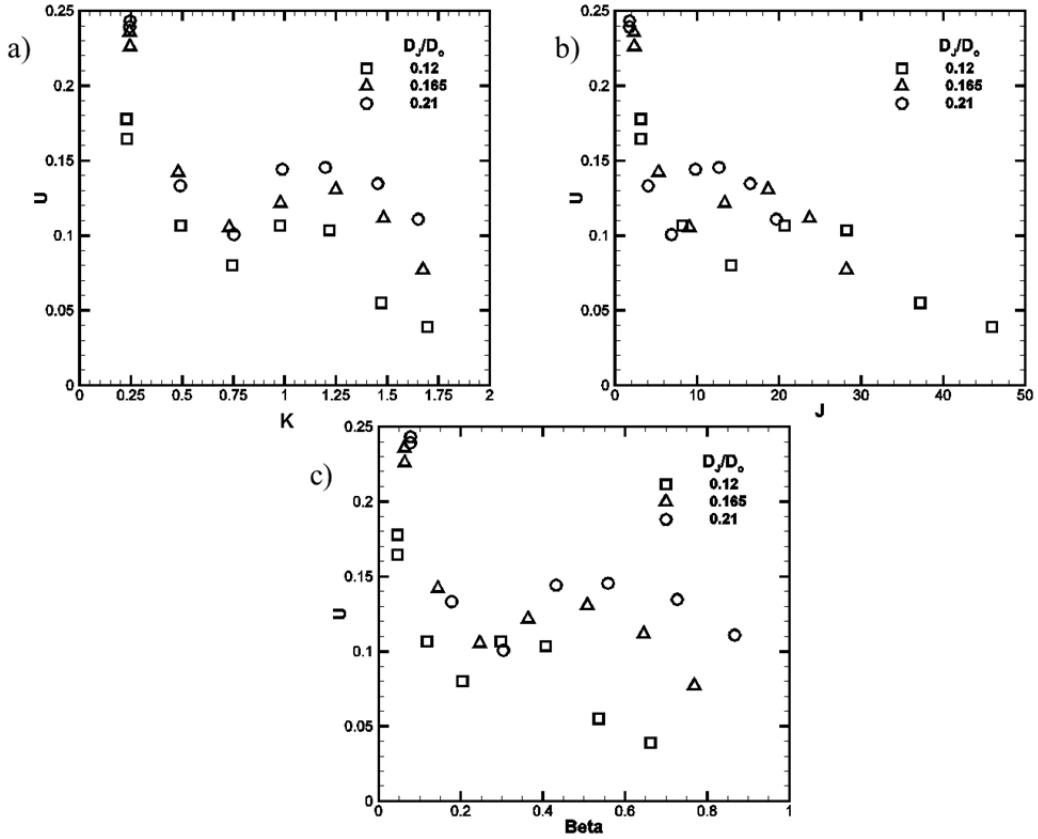

Figure 12: Mixture nonuniformity U for a single transverse jet scaled with a) K, b) momentum flux ratio J, and c) momentum ratio β.

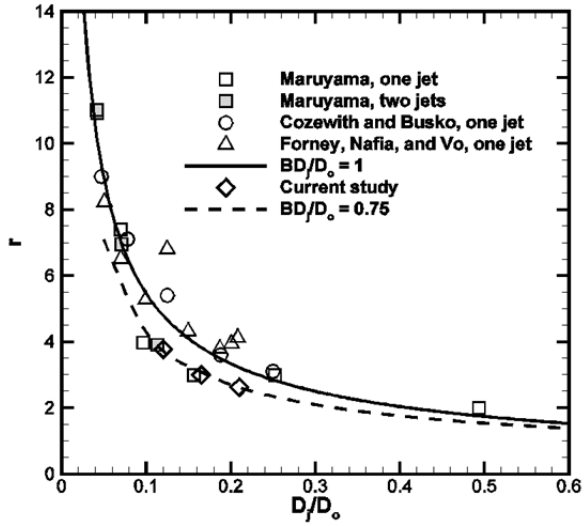

Figure 13: Optimum velocity ratio for a single confined transverse jet.

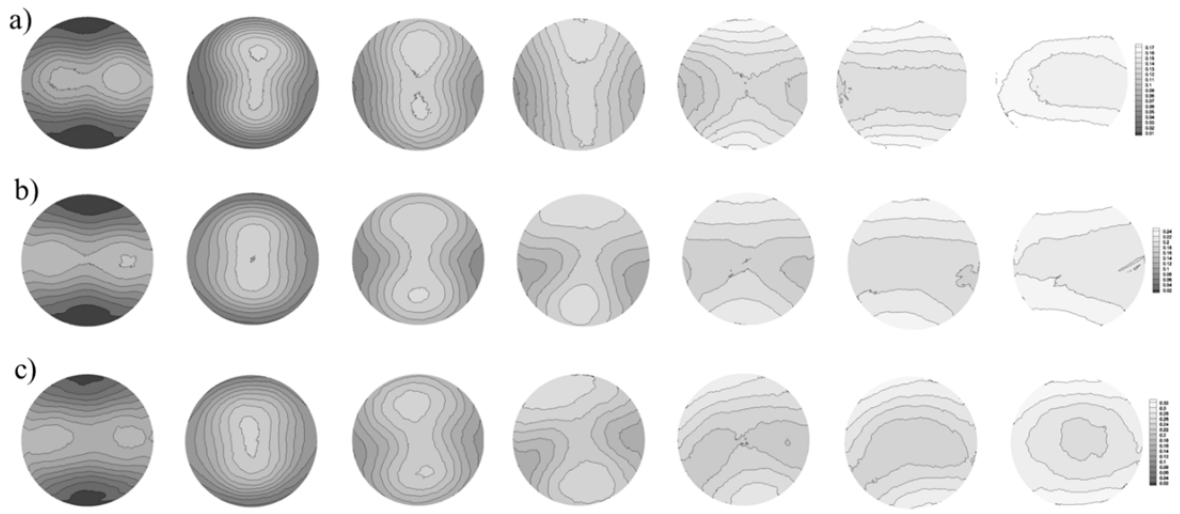

Figure 14: Mean mixture fraction distribution for two opposing transverse jets for D_j/D_o = a) 0.12, b) 0.165, and c) 0.21, with K increasing from left to right from 0.25 to 1.75 in increments of 0.25.

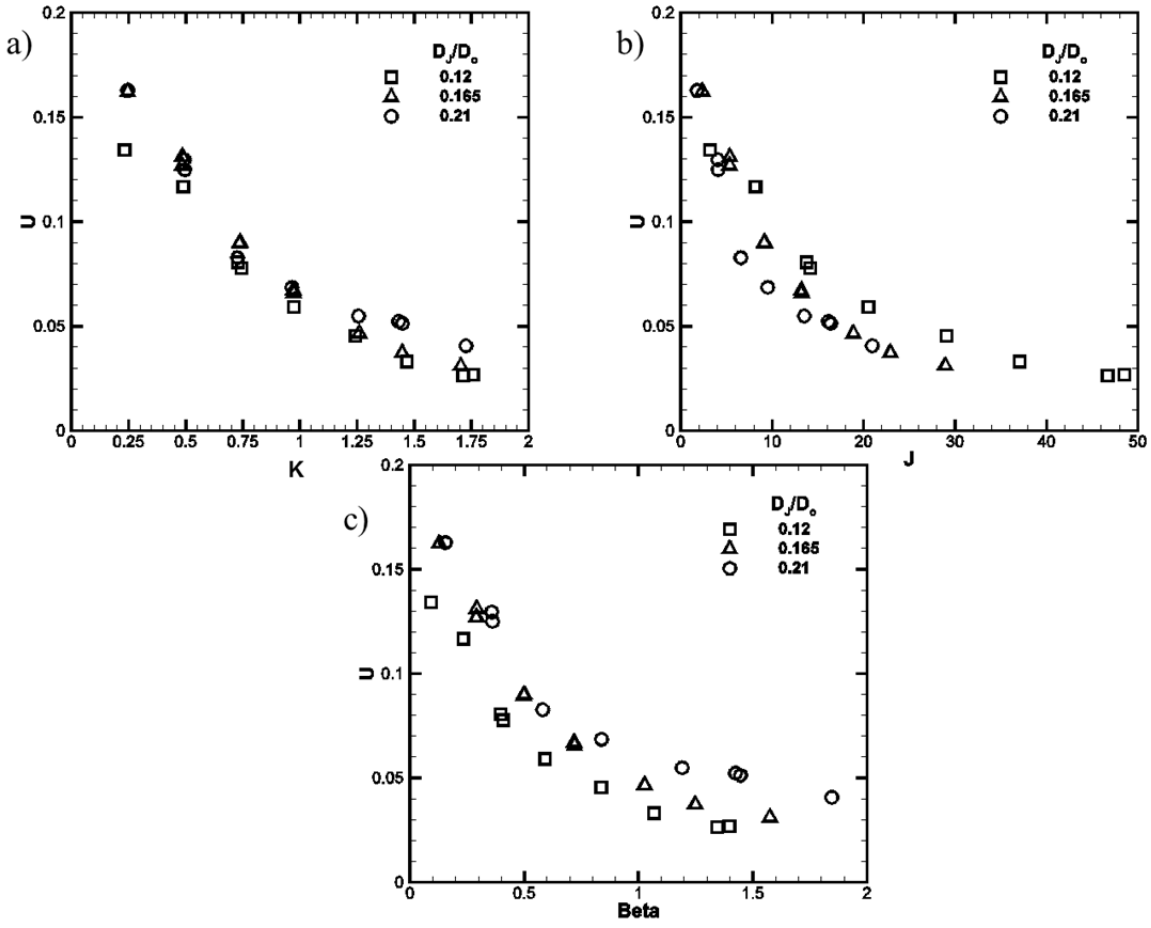

Figure 15: Mixture nonuniformity U for two opposed transverse jets scaled with a) K, b) momentum flux ratio J, and c) momentum ratio β.

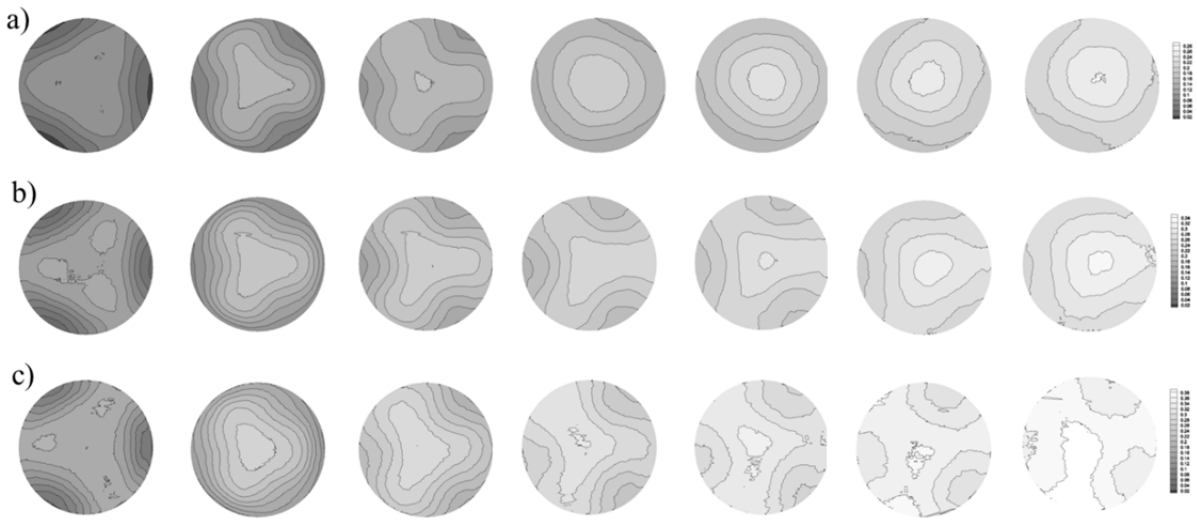

Figure 16: Mean mixture fraction distribution for three transverse jets for D_J/D_o = a) 0.12, b) 0.165, and c) 0.21, with K increasing from left to right from 0.25 to 1.75 in increments of 0.25.

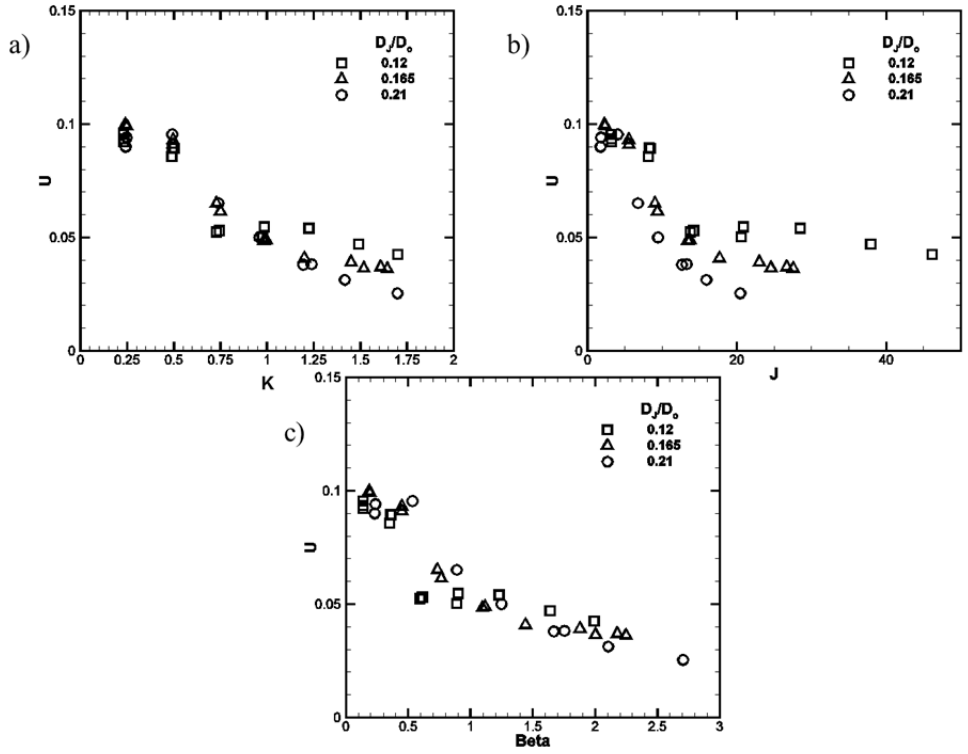

Figure 17: Mixture nonuniformity U for three transverse jets scaled with a) K, b) momentum flux ratio J, and c) momentum ratio β.

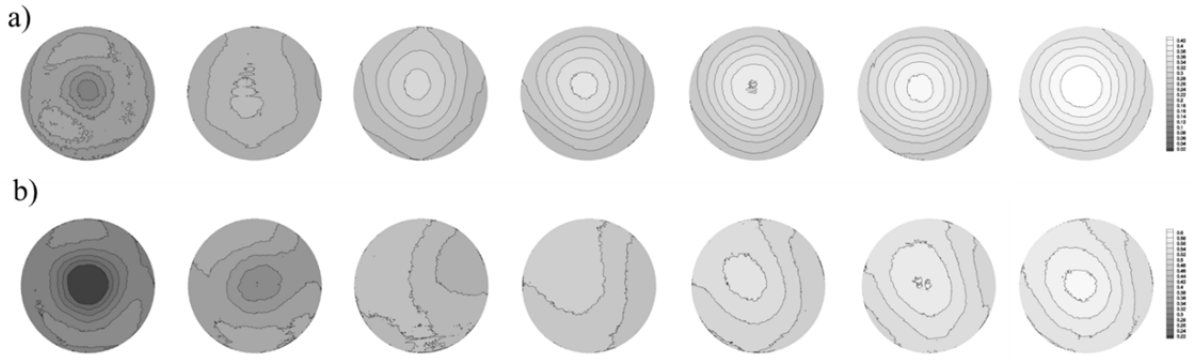

Figure 18: Mean mixture fraction distribution for six transverse jets for D_J/D_o = a) 0.12 and b) 0.21, with K increasing from left to right from 0.25 to 1.75 in increments of 0.25.

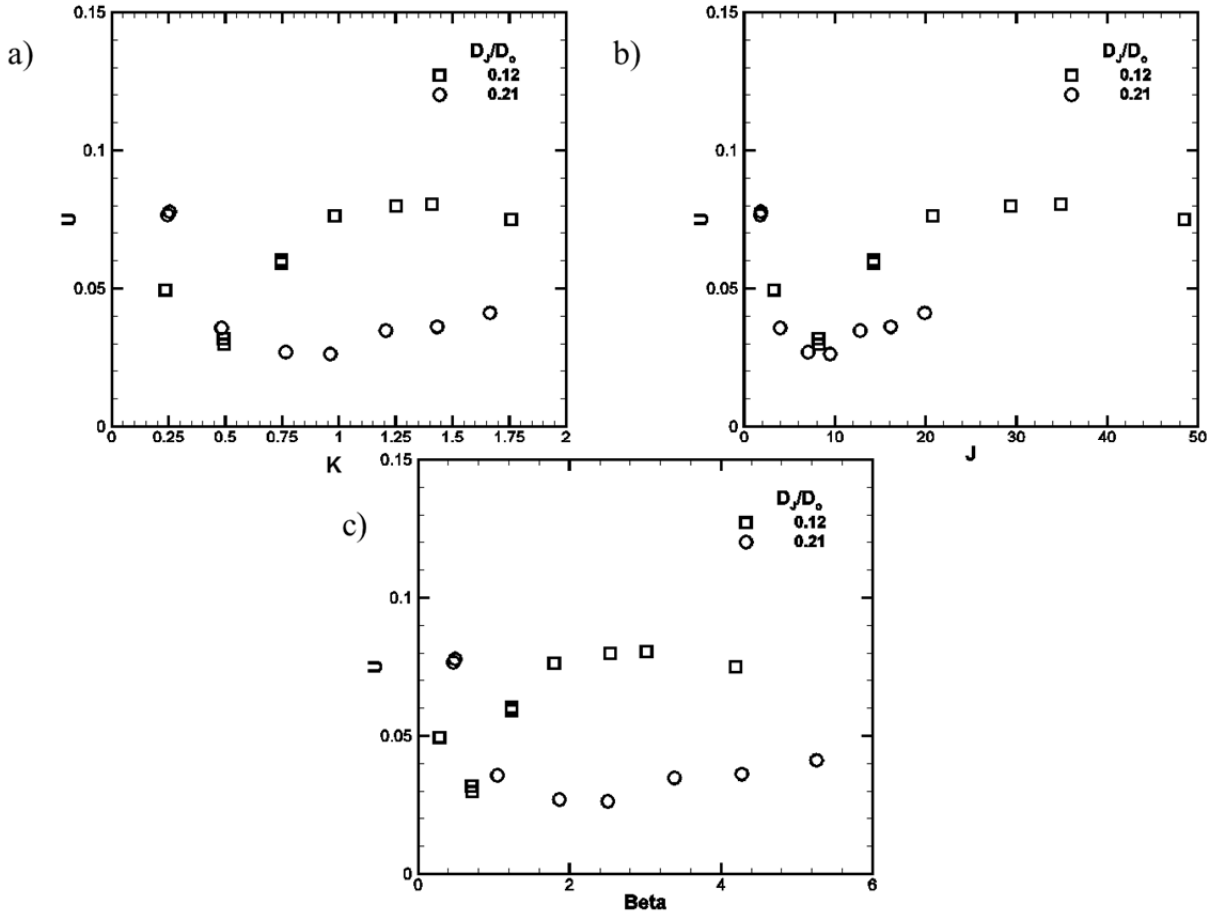

Figure 19: Mixture nonuniformity U for six transverse jets scaled with a) K, b) momentum flux ratio J, and c) momentum ratio β.

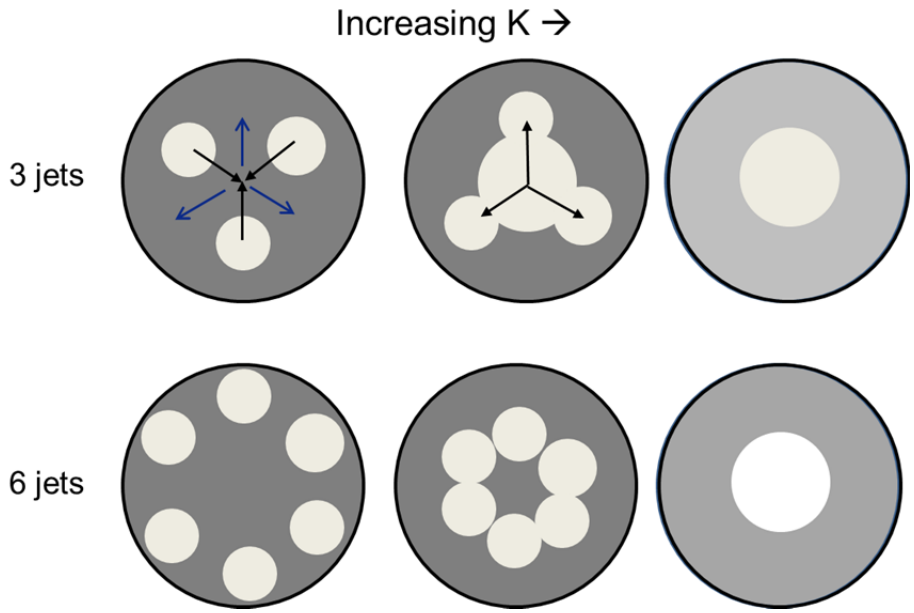

Figure 20: Mechanisms for three and six transverse jets.